Kinetics and coupled dynamics of dewetting and chemical reaction in Si/SiO2/Si system

Frédéric Leroy, D Landru, Fabien Cheynis, O Kononchuk, Pierre Müller, Stefano Curiotto

this manuscript has been published in Journal of Materials Science 55 (2020) 16074–16082

Kinetics and coupled dynamics of dewetting and chemical reaction in $Si/SiO_2/Si$ system

F. Leroy,[1,*] D. Landru,[2] F. Cheynis,[1] O. Kononchuk,[2] P. Müller,[1] and S. Curiotto[1]

[1] *Aix Marseille Univ, CNRS, CINAM, Marseille, France*

[2] *SOITEC, Parc Technol Fontaines, F-38190 Bernin, France*

(Dated: June 30, 2020)

Abstract

We report on the observation of a coupling between the dewetting of a Si layer on SiO_2 induced by surface/interface energy minimization and the etching between both materials due to the $Si+SiO_2 \longrightarrow 2\ SiO_g^{\uparrow}$ reaction. In the limit of a thin SiO_2 layer ($\leq$ 10 nm) sandwiched between a Si layer and a Si handle wafer, the front of Si dewetting and the front of SiO_2 etching coexist in a narrow region. The interplay between both phenomena gives rise to specific morphologies. We show that extended Si fingers formed by dewetting are stabilized with respect to Rayleigh Plateau type instability over tenth of microns thanks to a localized etching of the SiO_2 layer. The break up of this structure occurs abruptly by an unzipping process combining dewetting and etching phenomena. We also put in evidence that Si rings are created with a thin SiO_2 layer in the center. These processes are thermally activated with an activation energy of 2.4±0.5 eV and 4.0±0.5 eV respectively for dewetting and the etching reaction. All these results highlight the respective roles of wetting and etching in $Si/SiO_2/Si$ system dynamics and could be a stepping stone for the development of advanced processes based on Silicon-On-Insulator technology.

I. INTRODUCTION

Wetting of liquids on solids in reactive systems is of great importance with many industrial applications such as soldering or adhesion [1]. The kinetics of reactive wetting is affected by a number of factors like interfacial reactions, diffusion of constituents or dissolution of the substrate [2 and 3]. Under reaction the contact line dynamics can lead to complex behaviours such as oscillatory phenomenon of spreading and contraction [4–7], formation of reaction rings [8] or even droplet motion [9–11]. For example, the reaction-mediated spontaneous drift of millimeter-scale solid-state camphor particles on the surface of water has been known for several centuries [12]. In solid systems only scarce studies have explored the coupling between chemical reactions and wetting dynamics. For instance in metallic systems the alloying driving force can induce the self-propelled motion of solid Sn islands onto a Cu surface [13]. In the context of metal/oxide or semiconductor/oxide systems, solid state wetting properties may also be affected by interfacial redox reactions. For instance in the Si/SiO_2 couple, that plays a key role in the perspective of future devices based on Silicon-On-Insulator (SOI) technology [14–17], wetting and reactivity properties of the interface have been largely studied. Under moderate annealing ($\sim$ 1100-1300 K) SOI dewetting occurs by edge retraction (see Fig.1 and [18–24]), the expelled silicon accumulates in a receding rim that exhibits a capillary instability giving birth to elongated Si structures (called Si fingers). These fingers are in turn destabilized and periodically form 3D Si islands by a beading mechanism similar to a Rayleigh-Plateau instability. The driving force for this dewetting process arises from the surface/interface free energy gain. In solids mass transport is mediated by surface diffusion [25–27] whereas hydrodynamics dominates in liquid films [28–31]. This makes that the contact line with the substrate is particularly sensitive to the effect of the disjoining pressure in solid thin films whereas surface diffusion is much less affected [32]. Considering high temperature regimes ($\sim$ 1300 K) Si and SiO_2 solids are also known to react and form volatile $SiO_g^{\uparrow}$ molecules. This is perfectly illustrated when a SOI film is completely dewetted at 1000 K, then annealed at 1330 K: the reaction leads jointly to the consumption of the 3D Si islands and to the etching of nanopits in the SiO_2 layer [33 and 34].

In this article we analyze the combined effects of etching reaction and dewetting on SOI films in the high temperature regime. Their interplay gives complex front dynamics: (i)

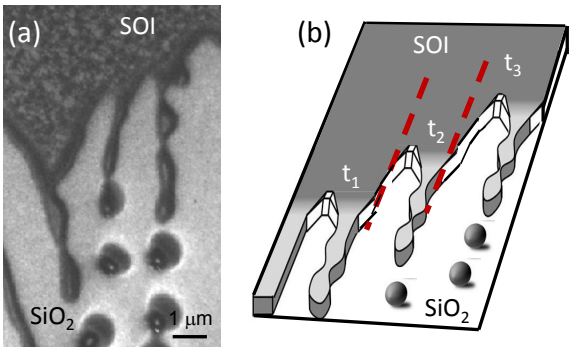

FIG. 1. (a) Low energy electron microscopy image of the dewetting of a SOI film (∼20 nm thick) at 1160 K. (b) sketch of the dewetting mechanism: a Si finger destabilizes by a lateral undulation (time t_1) that leads to beading and formation of a 3D Si island at its extremity (time t_2 ∼t_1+120 s). This process repeats periodically (time t_3 ∼t_1+240 s).

formation of extended Si fingers stabilized by lateral etching, (ii) Si fingers break up by an unzipping mechanism and (iii) formation of Si rings with a thin SiO_2 layer in the center. The etching and dewetting fronts dynamics are studied experimentally *in situ* and in real time by low energy electron microscopy (LEEM) and *ex situ* AFM measurements.

II. METHODS

The SOI wafers are originally fabricated at SOITEC (Bernin, France). They are cleaned and prepared in Ultra High Vacuum (UHV) conditions as described in Ref. [35]. The studied thickness is about 30 nm for the Si layer and 8 nm for the buried oxide layer (BOX) of SiO_2. Such thin structures are highly sensitive to Si layer dewetting and etching reaction between Si/SiO_2 under thermal annealing. In the temperature range $\sim 1300 - 1400$ K, a front of dewetting of the Si layer forms spontaneously onto a defect at the surface/interface and is followed by an etching reaction front. Their motion and morphology are recorded *in situ* and in real time (1 s per image) by low energy electron microscopy (LEEM) in the tilted bright field mode (electron energy: 4 eV). The characterization of the coupling between the etching and dewetting fronts dynamics is completed by *ex situ* analysis of the surface morphology by atomic force microscopy (AFM, PSIA-XE 100).

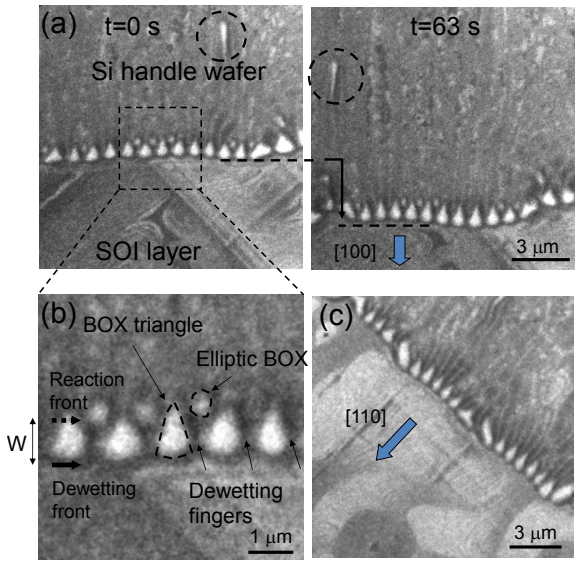

FIG. 2. (a) Sequence of two LEEM images of a thin SOI layer (30 nm) onto a BOX layer (8 nm) at 1370 K. The SOI dewetting front and the etching front Si/SiO_2 advance in the [100] direction (See Supplemental Material S1 at [URL will be inserted by publisher] for the complete movie). The Si handle wafer is on top of the image and the SOI layer is at the bottom. Dotted circles: SiO_2 layers moving opposite to the dewetting/etching front. The linear defects in the SOI layer (bottom right part of the image) occur due to remaining lateral temperature gradients during annealing. They have no influence on the fronts dynamics. (b) Close view of the area of coexistence of the dewetting front (black arrow) and reaction front (dashed arrow): The exposed SiO_2 layer has a bright contrast with a triangular or elliptical shape. Si fingers are formed in between triangular SiO_2 layers. (c) Same as (a) for an advancing front in the $\langle 110 \rangle$ direction.

III. RESULTS: INTERPLAY BETWEEN ETCHING REACTION AND DEWETTING FRONTS

A. Kinetics of fronts propagation

Figure 2(a) shows two LEEM images of the SOI (30 nm)/BOX (8 nm)/Si handle wafer during solid phase etching and dewetting at 1370 K. The SOI layer exhibits a black/white contrast coming from the $(1\times2)/(2\times1)$ surface reconstructions. The SOI dewetting front appears as an undulating grey line (fig. 2(b)) that separates the SOI layer and the underneath SiO_2 BOX layer (bright contrast). The fronts recede in a steady state at a constant velocity

of 53±5 nm.s^{-1}. If the front is aligned along the [100] direction very regular structures (1.5±0.1 μm period) occur whereas slightly more disordered ones can be observed when the front recedes in the [110] direction (Fig. 2(c)). A similar observation is obtained for Si(001) thin layer dewetting onto SiO_2 at lower temperature (1200 K) when etching reaction is negligible. The [100] front forms regular fingers by front edge instability as described by [36]. In the case of a [110] front, as there are two equivalent directions for the fingering instability ([100] and [010]), the competition between both degrades the long range order [23 and 24].

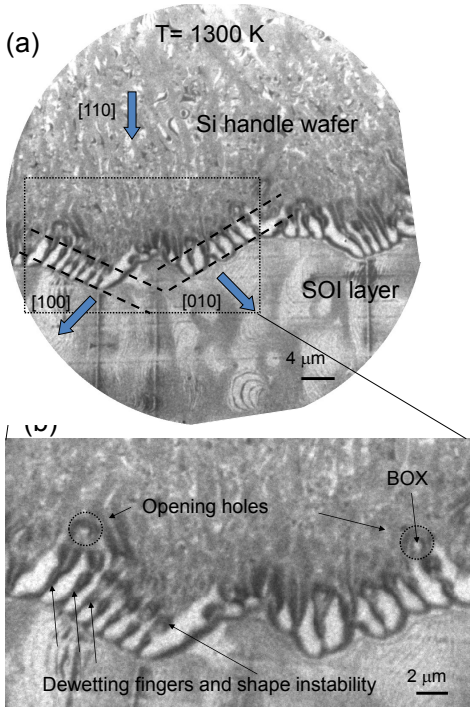

FIG. 3. (a) LEEM image of a SOI layer (30 nm) onto a BOX layer (8 nm) at 1300 K (See Supplemental Material S2 at [URL will be inserted by publisher] for the complete movie). The SOI dewetting front and the etching front Si/SiO_2 (middle) advance in the [110]. (b) Close view of the fronts: Si fingers onto SiO_2 layer are visible (black arrows) as well as circular holes in the Si layer (black dotted circles) exposing SiO_2.

As the SOI dewetting fronts recede (*via* fingers formation), the underlying SiO_2 BOX layer is exposed to vacuum (Fig. 2(b)). This free BOX layer shows triangular structures, the base pointing towards the SOI layer and the tip pointing in the direction of the Si handle wafer. We can infer that the edges of the triangles correspond to the reaction front between the remaining BOX layer and the Si handle wafer. As the front recedes in a steady state, the

decay of the BOX occurs by a constant etching reaction rate ($Si+SiO_2 \longrightarrow 2\ SiO_g^{\uparrow}$) localized at the Si/SiO_2/vacuum triple-line. To evaluate the activation energies of SOI dewetting E_d and etching reaction E_r we have studied the effect of the sample temperature on both kinetics (Fig. 3(a)-(b)). As the temperature decreases from 1370 K to 1300 K the fronts velocity v_f decreases from 53±5 nm.s^{-1} to 18±3 nm.s^{-1}, the extension of the free BOX layer W increases from 0.9±0.1 μm to 2.3±0.5 μm and the disappearance time t_d of the free BOX layer increases from 20±1 s to 125±20 s. The SOI front velocity v_f is only driven by SOI dewetting kinetics and can be written as $v_f \sim e^{-\frac{E_d}{kT}}$ assuming it is thermally activated. From the ratio of the velocities v_f at 1370 K and 1300 K, the dewetting activation energy is estimated as E_d=2.4±0.5 eV that is in perfect adequation with previous SOI dewetting studies [23] that show that Si surface diffusion is the dominant mechanism of mass transport mediating the dewetting process. The etching reaction activation energy E_r is not related to the reaction front velocity. Indeed the reaction occurs at the Si/SiO_2/vacuum triple-line and thus starts when the BOX is exposed to vacuum. Therefore the etching reaction activation energy has to be evaluated from the disappearance time $t_d \sim e^{\frac{E_r}{kT}}$ of the free BOX layer. Measurements of t_d at 1370 K and 1300 K provide an estimate of $E_r = 4.0 \pm 0.5$ eV. This is also in adequation with the activation energy reported by [33] from temperature dependent measurements of Si island decay kinetics onto SiO_2. At last we have also measured the width W of the exposed BOX layer with respect temperature. It is related both to dewetting and etching reaction activation energies as $W = v_f \times t_d \sim e^{\frac{E_r - E_d}{kT}}$. We measure that $E_r - E_d = 2.1 \pm 0.6$ eV. The large difference between the activation energies of Si dewetting and etching reaction makes that the width W of the free BOX layer decreases strongly with temperature as observed experimentally. At last let us note that despite the difference between both activation energies, the dewetting and etching fronts move at the same velocity (*i.e.* at the Si layer dewetting velocity, see supplementary material S1). This is due to the fact that the etching reaction occurs only when the BOX layer is exposed to vacuum, *i.e.* after the dewetting front passage. Then it takes a time t_d for the BOX layer to be completely etched which can be seen as a delay time for the etching front to progress behind the dewetting front.

This evaluation of the activation energies can also be completed with the quantitative analysis of the rate of etching reaction and dewetting front velocity. From the linear decrease of the BOX layer with time (triangular shape) the reaction rate $\nu_{reac} = \frac{dN}{dt}$ at the Si/SiO_2

contact line can be estimated (where N is the number of SiO_2 entities in the oxide layer). We calculate therefore $\nu_{reac} \approx 3.2 \times 10^3$ s^{-1} per SiO_2 entity at the contact line at 1370 K and $\nu_{reac} \approx 5 \times 10^2$ s^{-1} per SiO_2 entity at 1300 K (oxide layer thickness: 8 nm). This result compares to previous report [33] on the reaction rate of Si islands onto SiO_2 (3×10^2 s^{-1} per atom) in a slightly lower temperature regime. Concerning the dewetting velocity of SOI, Cheynis et al. [24] have shown that in the temperature range [1000 K - 1200 K] $v_f \simeq \frac{5.3\times10^{12}}{h^3 kT} e^{-2.0/kT}$ nm.s^{-1} where h is the SOI film height expressed in nm and kT is given in eV. Assuming this expression for a 30 nm thick film at 1370 K and 1300 K we obtain respectively v_f=74 nm.s^{-1} and v_f=31 nm.s^{-1} which gives the correct order of magnitude of the kinetics, the overestimation arising probably from a slightly too low activation energy in the modeling.

Beyond the description of the energetics of SiO_2 etching, figures 2(b) and 3(b) show also very specific structures that highlight a complex interplay between the dynamics of dewetting and etching. This interplay occurs because the timescale for the formation of fingers and 3D islands by dewetting is comparable to the timescale for the consumption of the BOX layer. We will focus on three main structures: (i) SiO_2 BOX layer of elliptic shape located in between two free BOX triangles and separated by Si (dotted ellipse in fig. 2(b), at 1370 K). (ii) Elongated free BOX structures crossing the surface from time to time in the direction opposite to the dewetting front (dotted circles in fig. 2(a)) with a large velocity (> 100 nm.s^{-1}). (iii) SOI islands with a ring shape and exposing a circular BOX layer in the middle (see fig. 3(b) at 1300 K). To understand all these structures we will describe in the following part the main stages of their formation and propose different scenarios with coupled etching and dewetting phenomena.

B. Coupled dynamics of dewetting and etching

a. ***Steady state elliptic shape BOX structure*** Figures 2(a)-(b) show LEEM images of a dewetting/reaction front moving along the [100] direction. The regularly spaced triangular BOX structures separate Si fingers that are short and perpendicular to the dewetting front. Some Si fingers are prolonged by BOX elliptic structures (dotted ellipse in fig. 2(b)) that are stable during the steady motion of the fronts (See complete movie S1 at [URL will be inserted by publisher]).

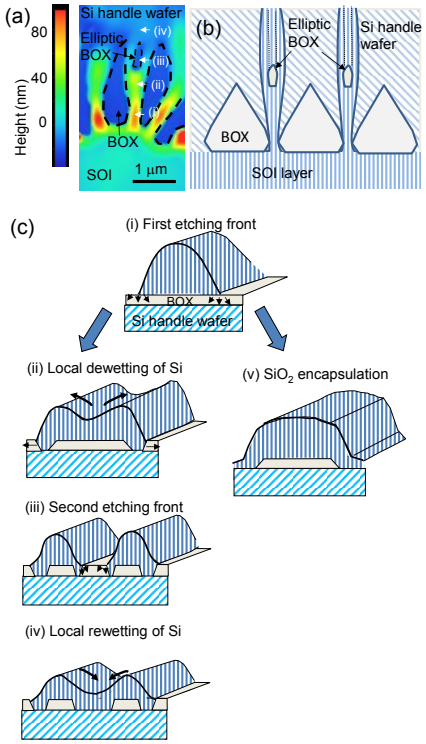

FIG. 4. (a) AFM image of the surface morphology of the front. Si fingers from the SOI layer separated by triangular shape BOX layers are visible. (i) to (iv) address the different steps of Si finger evolution (see scenario in (c)). (b) Scheme of the surface morphology considering elliptic holes (top view). (c) Scenario in four steps of the Si finger evolution: (i) Si finger formed by SOI layer dewetting and simultaneous SiO_2 BOX etching at the contact line. (ii) Complete lateral etching of the SiO_2 layer and contact between the Si finger (from SOI) and the Si handle wafer. Simultaneous lateral progression of the reaction front and Si mass shedding from the center of the finger. (iii) Splitting of the finger into two fingers and occurrence of new etching fronts with the free BOX. (iv) Complete etching of the inner SiO_2 BOX layer and rewetting of the SOI layer onto the Si handle wafer. (i)-(iv) are also sketched on AFM image in (a). (v) Scenario of direct BOX layer encapsulation (without finger splitting).

To analyze the morphology of these fronts combining dewetting and etching, figure 4(a) shows a typical AFM image. We can clearly distinguish the SOI layer (turquoise) and the Si fingers (yellow and red). The AFM image shows also the SiO_2 BOX layer (blue); it appears as extremely flat areas located in between Si fingers close to the SOI dewetting front. They have the same shape as those observed by LEEM (triangular structures in 2(c)). We can

also see from AFM that some Si fingers are unstable and split laterally into two branches exposing a small SiO_2 BOX layer ($\sim$500 nm) in between (elliptic shape) as the one measured by LEEM. From the combination of both methods, a scenario of the process is proposed (fig. 4(b)-(c)) based on the combined effects of SiO_2 BOX etching and wetting/dewetting of the SOI layer. The scenario involves four steps labelled (i) to (iv) that can be observed also by AFM (fig. 4(a)) as time lag is related to the spatial position with respect to the front. (i) First, a Si finger is formed by SOI dewetting on the SiO_2 BOX layer. This process is well known and arises from surface/interface energy minimization that kinetically destabilizes the receding front [37 and 38]. (ii) The Si finger formation results in the occurrence of a triple line between the freshly exposed SiO_2 BOX layer, the Si finger and vacuum. This contact line is very active for SiO_2 etching compared to SiO_2 dissolution through the SOI layer. Indeed, as shown by [39], the limiting mechanism for SiO_2 etching is the diffusion of dissolved O atoms created at the Si/SiO_2 interface. When O atoms reach the Si surface they combine to Si atoms and create volatile $SiO_g^{\uparrow}$ molecules. The diffusion time is therefore minimized when O atoms are directly formed at the triple line [33, 34, and 39]. The local etching thins locally the SiO_2 BOX layer ($\sim$8 nm) until the Si fingers meet the Si handle wafer. (iii) This has two consequences: (1) thermodynamically the Si finger tends to spread laterally on the Si handle wafer thanks to perfect wetting. (2) Kinetically the newly formed lateral etching front forces the finger to progress laterally. This enlargement of the fingers is visible in LEEM (fig. 3(b)) and AFM images (fig. 4(a)). This forced lateral spreading gives rise to a destabilization of the finger: it splits laterally in two parts with the occurrence of a newly exposed SiO_2 BOX layer in the middle. (iv) This SiO_2 layer is in turn the place for preferential etching at the triple line. When this SiO_2 layer in the middle is completely etched, the two Si fingers meet again and form a flattened structure that encapsulates the remaining SiO_2 BOX layers that are protected against further fast etching. When the splitting in two parts of the Si fingers does not occur, no elliptic SiO_2 layer is formed and another scenario with direct encapsulation of one SiO_2 BOX stripe occurs (see (v) in fig. 4(c)). This last scenario is clearly put in evidence in the unzipping process of Si fingers as detailed in the following.

b. ***Unzipping of Si fingers*** Figure 5(a) shows a sequence of LEEM images at 1370 K. We can observe a local anomaly at the reaction front edge: the triangular SiO_2 BOX layer is locally destabilized and this event suddenly generates a free SiO_2 layer that seems to

detach and propagate at high velocity (210±10 nm.s^{-1}) in the direction opposite to the front. To understand this process we have performed an *ex situ* analysis of the surface morphology by AFM. Fig. 5(c) shows an elongated silicon finger away from the front edge ($\sim$ 10 μm) which is hollowed out in the middle. A SiO_2 BOX layer is clearly observed at the bottom of this hollow as a very flat area surrounded by a Si rim and delimited by lateral trenches in the oxide layer (see height profile on fig. 5(c)). These very characteristic features of the SiO_2 BOX layer, etched locally by Si, have already been observed in the context of conventional SOI dewetting [23 and 39] and are found here everywhere at the front edge demonstrating unambiguously that the SiO_2 BOX can be present far away from the front. The proposed scenario is the following: The Si fingers formed by SOI dewetting locally etch the BOX layer on the lateral sides. When a Si finger reaches the Si handle wafer, the SiO_2 BOX layer may become encapsulated (see scenario (v) in fig. 4(c)) preventing further etching. This process is highly stabilized when the front recedes in the $\langle 100 \rangle$ direction resulting in the formation of extremely long SiO_2 BOX stripes ($>$ 30 μm) encapsulated into straight Si fingers. Contrary to conventional dewetting of Si/SiO_2, the encapsulation of a SiO_2 layer inside a Si structure prevents the dewetting of the Si fingers (fig. 5(b)-(1)). However if the dewetting front is destabilized and a finger detaches from the SOI layer edge (2), then a new triple line Si/BOX/vacuum appears. Lateral shedding of Si by dewetting is promoted (3). This process unzips the Si finger from the middle (hollowed Si finger) and creates two lateral rims of Si (4). Simultaneously the freshly exposed SiO_2 BOX layer is continuously etched on the lateral sides giving the impression of the propagation of a SiO_2 layer at the surface (5).

c. ***Si ring formation*** Figures 3(b) and 6(a) address a scenario occurring at slightly lower temperature (1300 K). At this temperature the width W at the front of the freshly exposed SiO_2 BOX layer is about 2 μm (dashed lines in fig. 3(a)) whereas it is about 0.9 μm at 1370 K. The width change arises because the activation energy for dewetting is lower (2.4 eV±0.5 eV) than for etching (4.0±0.5 eV as described previously). Therefore the Si fingers formed by dewetting are much longer and have now enough time to destabilize by a Rayleigh-Plateau type instability. However together with the usual formation of 3D Si islands, we also observe the formation of Si rings exposing in the middle a remaining SiO_2 BOX layer (see circles in fig. 3(b) and ref. [40]). This is also clearly seen by AFM (fig. 6(a)). Then this BOX layer in the middle of a Si ring is etched progressively and the ring

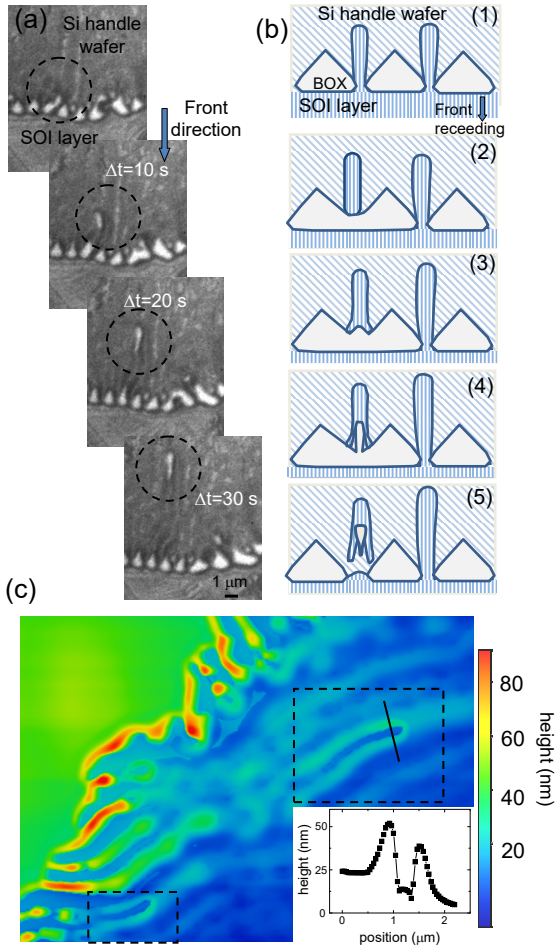

FIG. 5. (a) LEEM image sequence of Si/SiO_2 BOX front at 1370 K. Black dashed circles show the occurrence of a defect at the front that generates the linear propagation of a new front of SiO_2 BOX layer decomposition in the direction opposite to the dewetting front. (b) Scheme of the unzipping scenario of SOI finger with encapsulated SiO_2. The finger is destabilized at the front side. This event allows for the lateral dewetting of Si and splits the finger into two parts. This process progresses all along the finger over tenth of microns (unzipping process). Simultaneous etching of the newly exposed SiO_2 BOX layer.(c) AFM image (16×10 $mu m^2$) showing the morphology of this unzipping process (black dashed areas). Inset: profile of a silicon finger hollowed out in the middle (black line): Si lateral rim, trenches in the the SiO_2 layer at the contact line with Si and flat area of BOX in the middle.

shape smoothens giving a final rough Si surface morphology. We propose a scenario similar to the one described for Si fingers (fig. 4(c)) but adapted to 3D islands: (i) The 3D Si islands

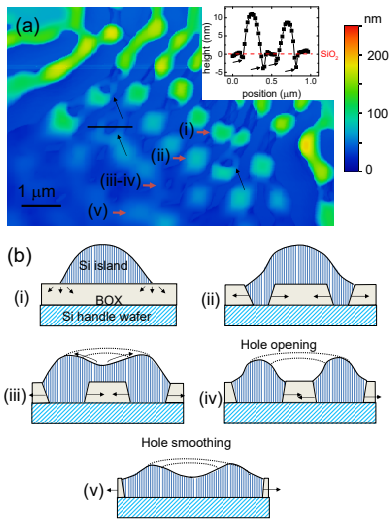

FIG. 6. (a) AFM image of the dewetting/reaction front (1300 K) obtained after quenching to RT. Elongated Si fingers are observed and agglomerate into 3D islands. The islands are unstable against Si rings formation (black arrow). Inset: profile of a circular hole (black line in the image) exposing a remaining SiO_2 BOX layer inside (BOX surface: red dashed line). Black arrows show the trenches in the BOX layer formed by local etching at the Si/SiO_2 contact lines. (b) Scenario of ring formation: (i) Si islands formed by dewetting and Si fingers. (ii) Local breaking through the SiO_2 layer and contact with the Si handle wafer. (iii) Radial progression of the reaction front and Si mass shedding from the center of the island. (iv) Opening of a hole into the center exposing the remaining SiO_2 BOX layer. (v) Etching of the SiO_2 BOX layer and spreading/smoothing of the Si layer.

formed by SOI finger dewetting instability [23 and 37] expose the BOX layer to vacuum. The circular contact line between the Si islands and the BOX layer is the place for preferential etching of the BOX layer. (ii) When the BOX layer is locally completely etched, the SOI layer and Si handle wafer are in contact and then the etching front progresses radially as for Si fingers. (iii) This process favors a mass transfer of Si from the center to the edge. (iv) This Si shedding destabilizes the compact island shape into a ring and a circular BOX layer

appears in the center as it was protected by the 3D island. This observation is similar to the one obtained in the context of liquid Si droplets onto SiO_2 (quartz) forming spontaneously a liquid Si torus [41]. (v) Then the inner SiO_2 layer progressively disappears by lateral etching and when it is completely etched the Si morphology smoothens.

IV. CONCLUSION

We have shown by *in situ* LEEM and *ex situ* AFM that the Si/SiO_2 interface in ultra thin SOI system can lead to different structures/morphologies depending on annealing conditions. The competition between (de)wetting and $Si+SiO_2 \longrightarrow 2\ SiO_g$ reaction kinetics makes possible to achieve steady state regimes where the dewetting front and the etching front coexist in a narrow space region. These regimes may create peculiar structures such as 1D thin SiO_2 BOX stripes encapsulated into crystalline Si fingers or Si rings with a SiO_2 BOX layer in the center. The formation of these structures follow different scenarios where the localization of the etching at the contact line between Si and SiO_2 and mass transfers induced by Si/SiO_2 wetting properties play key roles. Small modifications at the front edge may also lead to instabilities such as the fast unzipping of Si fingers with encapsulated SiO_2 BOX stripes. This analysis of the front dynamics is completed with a quantitative study of the energetics of the process. We show that dewetting and etching reaction are thermally activated with an activation energy respectively of 2.4 ± 0.5 eV and $4.0\ \pm0.5$ eV. To conclude, these results propose a general picture of the dynamics of $Si/SiO_2/Si$ interfaces at high temperature in the limit of a thin SiO_2 layer ($\leq$ 8 nm). We believe these results may initiate new approaches to fabricate specific structures based on SOI technology [42 and 43] and to prevent SOI dewetting processes by encapsulation approaches.

V. SUPPLEMENTARY MATERIALS

See supplementary materials for the complete movies of the dewetting and reacting processes.

ACKNOWLEDGMENTS

This work has been supported by the ANR grants LOTUS (ANR-13-BS04-0004-02) and HOLOLEEM (ANR-15-CE09-0012)

---

* leroy@cinam.univ-mrs.fr

[1] N Eustathopoulos. Dynamics of wetting in reactive metal/ceramic systems. *Acta Materiala*, 46(7):2319–2327, 1998.

[2] O. Dezellus and N. Eustathopoulos. Fundamental issues of reactive wetting by liquid metals. *Journal of Materials Science*, 45(16):4256–4264, 2010.

[3] Girish Kumar and K. Narayan Prabhu. Review of non-reactive and reactive wetting of liquids on surfaces. *Advances in Colloid and Interface Science*, 133(2):61–89, 2007.

[4] M Ohya, D Inoue, H Itoh, and T Ichinokawa. Oscillation of wettability of molten Cu islands on SiO_2. *Surface Science*, 369(1-3):169–176, 1996.

[5] T Ichinokawa, H Itoh, and Y Sakai. Behaviors of small molten metal islands on several substrates.

[6] H. Kanai, S. Sugihara, H. Yamaguchi, T. Uchimaru, N. Obata, T. Kikuchi, F. Kimura, and M. Ichinokura. Wetting and reaction between Si droplet and SiO_2 substrate. *Journal of Materials Science*, 42:9529, 2007.

[7] D. Wachsmuth, T. Gebensleben, D. Weiss, V. Becker, L. Alphei, and J. Becker. SiO gas emission and triple line dynamics of small silicon droplets on quartz. *J. Cryst. Growth*, 355, 2012.

[8] E. Saiz, A.P. Tomsia, and K. Suganuma. Wetting and strength issues at Al/alpha-alumina interfaces. *Journal of the European Ceramic Society*, 23(15):2787–2796, 2003.

[9] S. Curiotto, F. Leroy, F. Cheynis, and P. Müller. Self-propelled motion of Au-Si droplets on Si(111) mediated by monoatomic step dissolution. *Surface Science*, 632:1–8, 2015.

[10] S. Curiotto, F. Leroy, F. Cheynis, and P. Müller. In-plane Si nanowire growth mechanism in absence of external Si flux. *Nano Letters*, 15:4788, 2015.

[11] S. Curiotto, F. Leroy, F. Cheynis, and P. Müller. Surface-dependent scenarios for dissolution-driven motion of growing droplets. *Scientific Reports*, 7:902, 2017.

[12] Satoshi Nakata and Yuko Hayashima. Spontaneous dancing of a camphor scraping. *J. Chem. Soc., Faraday Trans.*, 94:3655–3658, 1998.

[13] A. K. Schmid, N. C. Bartelt, and R. Q. Hwang. Alloying at surfaces by the migration of reactive two-dimensional islands. *Science*, 290:1561, 2000.

[14] M. Bollani, M. Salvalaglio, A. Benali, and et al. Templated dewetting of single-crystal sub-millimeter-long nanowires and on-chip silicon circuits. *Nature Communications*, 10:5632, 2019.

[15] Meher Naffouti, Rainer Backofen, Marco Salvalaglio, Thomas Bottein, Mario Lodari, Axel Voigt, Thomas David, Abdelmalek Benkouider, Ibtissem Fraj, Luc Favre, Antoine Ronda, Isabelle Berbezier, David Grosso, Marco Abbarchi, and Monica Bollani. Complex dewetting scenarios of ultrathin silicon films for large-scale nanoarchitectures. *Sci. Adv.*, 3(11), 2017.

[16] F. Leroy, L. Borowik, F. Cheynis, Y. Almadori, S. Curiotto, M. Trautmann, J. C. Barbe, and P. Müller. *Surf. Sci. Rep.*, 71(2):391–409, 2016.

[17] M. Trautmann, F. Cheynis, F. Leroy, S. Curiotto, O. Pierre-Louis, and P. Muller. Dewetting of patterned solid films: Towards a predictive modelling approach. *Appl. Phys. Lett.*, 110:263105, 2017.

[18] Y. Ono, M. Nagase, M. Tabe, and Y. Takahashi. *Jap. J. Appl. Phys.*, 34:1728, 1995.

[19] R. Nuryadi, Y. Ishikawa, and M. Tabe. Formation and ordering of self-assembled si islands by ultrahigh vacuum annealing of ultrathin bonded silicon-on-insulator structure. *Appl. Surf. Sci.*, 159-160:121, 2000.

[20] R. Nuryadi, Y. Ishikawa, Y. Ono, and M. Tabe. Thermal agglomeration of single-crystalline Si layer on buried SiO_2 in ultrahigh vacuum. *J. Vac. Sci. Technol. B*, 20:167, 2002.

[21] B. Legrand, V. Agache, J. P. Nys, V. Senez, and D. Stiénvenard. Formation of silicon islands on a silicon on insulator substrate upon thermal annealing. *Appl. Phys. Lett.*, 76:3271, 2000.

[22] B. Legrand, V. Agache, T Mélin, J. P. Nys, V. Senez, and D. Stiévenard. Thermally assisted formation of silicon islands on a silicon-on-insulator substrate. *J. Appl. Phys.*, 91:106, 2002.

[23] E. Bussmann, F. Cheynis, F. Leroy, P. Müller, and O. Pierre-Louis. Dynamics of solid thin-film dewetting in the silicon-on-insulator system. *New J. Phys.*, 13:043017, 2011.

[24] F. Cheynis, E. Bussmann, F. Leroy, T. Passanante, and P. Müller. Dewetting dynamics of silicon-on-insulator thin films. *Phys. Rev. B.*, 84:245439, 2011.

[25] W. W. Mullins. Theory of thermal grooving. *Journal of Applied Physics*, 28(3):333–339, 1957.

[26] H Wong, PW Voorhees, MJ Miksis, and SH Davis. Periodic mass shedding of a retracting solid film step. *Acta Materiala*, 48(8):1719–1728, 2000.

[27] Yan Wang, Wei Jiang, Weizhu Bao, and David J. Srolovitz. Sharp interface model for solid-state dewetting problems with weakly anisotropic surface energies. *Physucal Review B*, 91(4), 2015.

[28] G Reiter. Dewetting of thin polymer-films. *Physical Review Letter*, 68(1):75–78, 1992.

[29] Rabibrata Mukherjee and Ashutosh Sharma. Instability, self-organization and pattern formation in thin soft films. *Soft Matter*, 11(45):8717–8740, 2015.

[30] Nandini Bhandaru, Anuja Das, Namrata Salunke, and Rabibrata Mukherjee. Ordered Alternating Binary Polymer Nanodroplet Array by Sequential Spin Dewetting. *Nano Letters*, 14(12):7009–7016, 2014.

[31] Palash Dhara, Nandini Bhandaru, Anuja Das, and Rabibrata Mukherjee. Transition from Spin Dewetting to continuous film in spin coating of Liquid Crystal 5CB. *Scientific Reports*, 8, 2018.

[32] Ashwani K. Tripathi and Olivier Pierre-Louis. Disjoining-pressure-induced acceleration of mass shedding in solid-state dewetting. *Physical Review E*, 101(4), 2020.

[33] F. Leroy, Y. Saito, F. Cheynis, E. Bussmann, O. Pierre-Louis, and P. Müller. Nonequilibrium diffusion of reactive solid islands. *Phys. Rev. B*, 89:235406, 2014.

[34] F. Leroy, Y. Saito, S. Curiotto, F. Cheynis, O. Pierre-Louis, and P. Müller. Shape transition in nano-pits after solid-phase etching of SiO_2 by Si islands. *Applied Physics Letters*, 106(19):191601, 2015.

[35] E. Bussmann, F. Cheynis, F. Leroy, and P. Müller. Thermal instability of silicon-on-insulator thin films measured by low-energy electron microscopy. *IOP Conf. Ser. Mat. Sci. and Eng.*, 12:012016, 2010.

[36] F. Leroy, F. Cheynis, T. Passanante, and P. Müller. Dynamics, anisotropy, and stability of silicon-on-insulator dewetting fronts. *Phys. Rev. B*, 85:195414, 2012.

[37] David T. Danielson, Daniel K. Sparacin, Jurgen Michel, and Lionel C. Kimerling. Surface-energy-driven dewetting theory of silicon-on-insulator agglomeration. *Journal of Applied Physics*, 100(8), 2006.

[38] E. Dornel, J-C. Barbé, F. de Crécy, G. Lacolle, and J. Eymery. Surface diffusion dewetting of thin solid films: Numerical method and application to Si/SiO_2. *Phys. Rev. B.*

[39] K. Sudoh and M. Naito. Interfacial reaction of Si islands on SiO_2 during high-temperature annealing. *J. Appl. Phys.*, 108:083520, 2010.

[40] S. Curiotto, F. Leroy, F. Cheynis, and P. Müller. Oxygen-induced inhibition of silicon-on-insulator dewetting. *Applied Physics Letters*, 104(6):061603, 2014.

[41] L. D. Alphei, R. Grotjahn, V. Becker, R. Janhsen, M. Douvidzon, and J. A. Becker. Reaction enhanced wetting of quartz by silicon droplets and its instabilities. *J. Materials Science*, 48(21):7350–7359, 2013.

[42] L. Borowik, J.-C. Barbé, E. Bussmann, F. Cheynis, F. Leroy, D. Mariolle, and P. Müller. Method for making semi-conductor nanocrystals, Nov. 8, 2012. Publication Number: US2012282758.

[43] L. Borowik, J.-C. Barbé, E. Bussmann, F. Cheynis, F. Leroy, D. Mariolle, and P. Müller. Method for making semi-conductor nanocrystals oriented along a predefined direction, Nov. 8, 2012. Publication Number: US2012282759.